Vascular endothelial growth factor receptor 2 inhibition in-vivo affects tumor vasculature in a tumor type-dependent way and downregulates vascular endothelial growth factor receptor 2 protein without a prominent role for miR-296

Elise Langenkamp[a], Peter J. Zwiers[a], Henk E. Moorlag[a], William P. Leenders[b], Brad St. Croix[c] and Grietje Molema[a]

The precise molecular effects that antiangiogenic drugs exert on tumor vasculature remain to be poorly understood. We therefore set out to investigate the molecular and architectural changes that occur in the vasculature of two different tumor types that both respond to vascular endothelial growth factor receptor 2 (VEGFR2) inhibitor therapy. Mice bearing Lewis lung carcinoma (LLC) or B16.F10 melanoma were treated with vandetanib (ZD6474), a VEGFR2/epidermal growth factor receptor (EGFR)/REarranged during Transfection (RET) kinase inhibitor, resulting in a significant 80% reduction in tumor outgrowth. Although in LLC the vascular density was not affected by vandetanib treatment, it was significantly decreased in B16.F10. In LLC, vandetanib treatment induced a shift in vascular gene expression toward stabilization, as demonstrated by upregulation of Tie2 and N-cadherin and downregulation of Ang2 and integrin β3. In contrast, only eNOS and P-selectin responded to vandetanib treatment in B16.F10 vasculature. Strikingly, vandetanib reduced protein expression of VEGFR2 in both models, whereas mRNA remained unaffected. Analysis of miR-296 expression allowed us to exclude a role for the recently proposed microRNA-296 in VEGFR2 posttranslational control in LLC and B16.F10 *in vivo*. Our data demonstrate that VEGFR2/EGFR inhibition through vandetanib slows down both LLC and B16.F10 tumor growth. Yet, the underlying molecular changes in the vasculature that orchestrate the antitumor effect differ between tumor types. Importantly, in both models, vandetanib treatment induced loss of its pharmacological target, which was not directly related to miR-296 expression. Validation of our observations in tumor biopsies from VEGFR2 inhibitor-treated patients will be essential to unravel the effects of VEGFR2 inhibitor therapy on tumor vasculature in relation to therapeutic efficacy. *Anti-Cancer Drugs* 23:161–172 © 2012 Wolters Kluwer Health | Lippincott Williams & Wilkins.

Anti-Cancer Drugs 2012, **23**:161–172

Keywords: receptor tyrosine kinase inhibitors, tumor angiogenesis, vascular gene expression, vascular stabilization, vascular endothelial growth factor receptor 2 inhibition

[a]Department of Pathology and Medical Biology, Medical Biology Section, University Medical Center Groningen, University of Groningen, Groningen, The Netherlands, [b]Department of Pathology, University Medical Center Nijmegen, Nijmegen, The Netherlands and [c]Mouse Cancer Genetics Program, Tumor Angiogenesis Section, National Cancer Institute at Frederick, Maryland, USA

Correspondence to Dr Grietje Molema, PhD, Department of Pathology and Medical Biology, Medical Biology Section, University Medical Center Groningen, University of Groningen, Internal Postal Code EA11, Hanzeplein 1, Groningen 9713 GZ, The Netherlands
Tel: +31 5 03618043; fax: +31 5 03619911;
e-mail: g.molema01@umcg.nl

Present address: Elise Langenkamp, Uppsala University, Rudbeck Laboratory, Department of Immunology, Genetics and Pathology, Uppsala, Sweden.

Received 14 July 2011 **Revised form accepted** 3 October 2011

Introduction

For metastasis and growth, many tumors depend on angiogenesis, a tightly regulated process in which vascular endothelial growth factor (VEGF) plays a key regulatory role [1]. Indeed, high levels of VEGF alone are capable of initiating angiogenesis in a quiescent vasculature [2], and in most cancers VEGF overexpression is associated with disease progression [3], which makes VEGF an attractive target for antiangiogenic therapy. Currently, five inhibitors of the VEGF pathway have been approved by the Food and Drug Administration for use in cancer therapy [4]. Importantly, the cellular and molecular mechanisms that underlie efficient tumor growth inhibition through VEGF inhibitor therapy remain unknown. Several mechanisms of action have been proposed that contribute to the effect of VEGF-blocking agents, including inhibition of neovessel growth, blockade of incorporation of endothelial progenitor cells, induction of endothelial cell apoptosis, and vascular normalization [5,6].

In many preclinical models, inhibition of tumor growth by inhibitors of VEGF signaling has been related to a decrease in microvascular density [7–9]. Yet, the changes in vascular gene expression upon VEGFR2 inhibition that orchestrate the tumor growth inhibitory effect in these models remain largely unknown. Studies in various in-vitro and in-vivo neovascularization models have shown that VEGF signaling upregulates the expression of many regulators of the angiogenic process, such as integrin αvβ3, the zinc finger transcription factor early growth response 3, the NR4A family of orphan nuclear receptors, matrix metalloproteinases, NO synthases, Robo1, Nur77, Tie2, and the Notch/Dll4/Jagged-1 signaling family, while downregulating the expression of Inter-Cellular Adhesion

0959-4973 DOI: 10.1097/CAD.0b013e32834dc279

Molecule (ICAM) and Vascular Cell Adhesion Molecule (VCAM) [10–16]. The consequences of inhibition of VEGF signaling for endothelial gene expression patterns *in vivo* remain largely unknown.

In the present study, we aimed to identify the molecular changes that occur in the vasculature of Lewis lung carcinoma (LLC) and B16.F10 melanoma upon anti-angiogenic VEGFR2 inhibitor therapy. As a model antiangiogenic compound, we used the small molecule VEGFR2 tyrosine kinase inhibitor vandetanib (ZD6474), which exerts its effect by preventing binding of ATP to the ATP-binding pocket of the receptor, thereby inhibiting autophosphorylation of the receptor dimers [17]. Vandetanib has additional affinity for epidermal growth factor receptor (EGFR) and REarranged during Transfection (RET) [18], and is currently in clinical trials for medullary thyroid cancer and a range of other tumor types [19]. We treated LLC and B16.F10 melanoma-bearing mice with vandetanib, monitored tumor growth during the course of therapy, and analyzed the consequences for vascular architecture and density. Interestingly, we found that vandetanib-enforced tumor growth inhibition was accompanied by a significant decrease in the vascular density in the B16.F10 melanoma model, whereas in LLC the overall vascular surface area remained unaffected. To unravel the molecular basis for this difference in vascular behavior, we set out to unravel the compartmentalized effects of vandetanib on gene expression in the vasculature of both models, which was isolated by laser microdissection before transcriptional profiling. On the basis of the observed changes in vascular gene expression, we assessed the pattern of pericyte coverage in both models. Furthermore, we investigated the localization of expression of the pharmacological targets of vandetanib, and found that in both models vandetanib decreased protein levels of VEGFR2. As the VEGFR2 mRNA level was not affected by therapy, we assessed whether the recently proposed VEGFR2-controlling microRNA-296 has a role in vandetanib-induced VEGFR2 protein loss.

Materials and methods

Tumor cell culture and animal studies

B16.F10 murine melanoma cells were cultured in Dulbecco's Modified Eagle Medium (Biowhittaker, Verviers, Belgium) supplemented with 10% fetal calf serum (Hyclone, Perbio Science, Etten-Leur, The Netherlands), 2 mmol/l of L-glutamine (Biowhittaker), and 1% gentamicin (Biowhittaker). Murine LLC cells (ATCC, Manassas, Virginia, USA) were cultured in Dulbecco's Modified Eagle Medium (Cellgro Mediatech, Manassas, Virginia, USA) supplemented with 5% fetal calf serum, 100 IU/ml of penicillin, and 100 μg/ml of streptomycin (Cellgro Mediatech). Both cell lines were kept at 37°C and 5% CO_2/95% air in a humidified incubator.

C57bl/6 male mice (Charles River, Frederick, Maryland, USA; and Harlan, Zeist, The Netherlands) were subcutaneously injected with 500 000 LLC cells or 100 000 B16.F10 cells in 100 μl of phosphate-buffered saline. Tumors were measured every other day using calipers, and volume was calculated according to the following formula: tumor volume $= 0.52 \times \text{length} \times \text{width}^2$, with 'width' being the shorter of the two parameters. When tumors appeared palpable, mice were randomly distributed into two groups, receiving intraperitoneal injections with vandetanib (ZD6474; a kind gift from AstraZeneca, Macclesfield, UK) at 80 mg/kg in 5% arabic gum [20] or with vehicle alone, once a day. As for the LLC-bearing animals, injection with vandetanib was omitted at days 3 and 8 after the start of treatment to prevent further weight loss during the course of therapy. After 9–11 days of treatment, the animals were killed under anesthesia by inhalation of isoflurane/O_2 or by CO_2 euthanasia, and tumors were excised, immediately snap-frozen in liquid N_2, and stored at –80°C until further analysis.

All experiments were carried out in accordance with the Animal Care and Use guidelines by the National Cancer Institute at Frederick and the University of Groningen.

Immunohistochemical and immunofluorescent staining of tumor tissues

Immunohistochemical detection of CD31, VEGFR2, and EGFR in acetone-fixed, 5 or 10-μm cryostat-cut tumor sections was carried out using the Dako Envision System-HRP kit (Dako Cytomation, Glostrup, Denmark) according to the supplier's protocol. We used primary antibodies to CD31 (BD Pharmingen; clone MEC13.3), Flk1, and EGFR (both from R&D, Minneapolis, Minnesota, USA). Detection was carried out with Rabbit-anti-Rat IgG (H + L; Vector Labs, Burlingame, California, USA) or HRP-labeled Rabbit-anti-Goat IgG (Dako), and after subsequent incubation with an anti-rabbit HRP-conjugated polymer for 30 min, peroxidase activity was detected with 3-amino-9-ethylcarbazole complex and sections were counterstained with Mayer's hematoxylin (Merck, Darmstadt, Germany). Sections were embedded in Kaisers Glycerin (Merck) and examined using a Leica DMLB microscope (Leica, Wetzlar, Germany) equipped with Leica DFC 420C camera, and the Leica Qwin V3.5.1 software. The percentage of CD31-positive surface area was quantified by morphometric analysis using the same software package.

To visualize pericytes, sections were double stained with antibodies to either αSMA (Cy3 labeled; Sigma Aldrich, Steinheim, Germany) or desmin (Abcam, Cambridge, UK), together with antibodies against CD31. Subsequently, sections were incubated with Alexa fluor 568-conjugated Goat-anti-Rabbit IgG to detect desmin and Alexa fluor 488-conjugated Goat-anti-Rat IgG to detect CD31 (both H + L, Molecular Probes Invitrogen Detection Technologies, Eugene, Oregon, USA), and

nuclear counterstaining was carried out using DAPI (F. Hoffmann-La Roche Ltd, Basel, Switzerland). Autofluorescence was reduced by incubation in 0.1% Sudan Black (Sigma-Aldrich) in 70% ethanol for 30 min, after which the sections were embedded in Citifluor (Citifluor Ltd., London, UK) and examined using a fluorescence microscope (DM RXA, Leica) and Leica Qwin V3 software.

mRNA extraction from whole-tumor samples

Extraction of total RNA from cryostat-cut sections of LLC and B16.F10 tissue as a whole was carried out according to the protocol of RNeasy Mini Plus kit or microRNeasy Mini Kit (both from Qiagen, Leusden, The Netherlands; the latter was used to isolate total RNA including microRNAs). RNA was analyzed qualitatively by gel electrophoresis and quantitatively by Nanodrop ND-100 spectrophotometry (NanoDrop Technologies, Rockland, Delaware, USA) and was consistently found to be intact and protein free.

Laser microdissection of B16.F10 and Lewis lung carcinoma tumor vasculature

Cryosections of 9 µm from B16.F10 tumors mounted on polyethylene–naphtalene membranes attached to normal glass slides (P.A.L.M. Microlaser Technology AG, Bernried, Germany) were fixed in acetone and stained with Mayer's hematoxylin, washed with diethyl pyrocarbonate-treated water, and were air dried. Tumor vascular segments ($1–2 \times 10^6$ µm^2 surface area, including vessel lumen area) were recognized on the basis of a visible lumen and were microdissected using the LMD6000 Laser Microdissection system (Leica). Blood vessels growing in LLC generally do not contain a visible lumen and are therefore not identifiable by hematoxylin staining. For this, we stained 9-µm acetone-fixed cryosections of LLC with a Goat antibody to Collagen IV (Southern Biotech, Birmingham, Alabama, USA) that was labeled with an Alexa488 conjugate using the Zenon Alexa fluor 488 Goat IgG labeling kit (Invitrogen, Carlsbad, California, USA). Sections were washed twice with phosphate-buffered saline and air dried before microdissection.

Total RNA was extracted according to the protocol of the RNeasy Microkit or microRNeasy Mini Kit (Qiagen) and was reverse transcribed for use in quantitative PCR as described below.

Gene expression analysis by quantitative reverse transcriptase polymerase chain reaction

Total RNA was reverse transcribed as described previously [21] using Superscript III Reverse Transcriptase (Invitrogen) in a 20-µl final volume containing 250 ng of random hexamers (Promega, Madison, Wisconsin, USA) and 40 units of RNase OUT inhibitor (Invitrogen). mRNA expression analysis was carried out in a real-time PCR-based, custom-designed, low-density array setup (Applied Biosystems, Foster City, California, USA). The low-density array was designed with exon-overlapping primers and minor groove-binding probes of 45 genes selected for their involvement in angiogenesis, inflammation, and basic influence on endothelial cell behavior, and of GAPDH as housekeeping gene. The low-density array card was processed according to the supplier's protocol and analyzed in an ABI PRISM 7900HT Sequence Detector System (Applied Biosystems).

For selection of genes, real-time PCR was carried out in duplicate per sample with 1 µl cDNA per reaction in TaqMan PCR MasterMix in a total volume of 10 µl, with primer-probe sets (where appropriate corresponding to the ones prespotted on the low-density array cards) being purchased as Assay-on-Demand from Applied Biosystems (Nieuwekerk a/d IJssel, The Netherlands).

MicroRNA expression analysis

Isolated microRNA was transcribed using the Taqman MicroRNA Reverse Transcription Kit (Applied Biosystems) in a 15-µl final volume according to the suppliers' protocol. MicroRNA-126 and microRNA-296 expression analyses were carried out in a real-time PCR-based setup with 1 µl cDNA per reaction in TaqMan PCR MasterMix in a total volume of 10 µl, with primer-probe sets (MicroRNA assays) being purchased from Applied Biosystems (Nieuwekerk a/d IJssel, The Netherlands). Small nuclear RNA sno-202 (Applied Biosystems) was assayed as an internal control.

Statistics

Statistical significance of the observed differences was addressed by means of Student's *t*-test or analysis of variance, with post-hoc comparison using the Bonferroni correction on the mean of duplicate quantitative reverse transcriptase polymerase chain reaction analyses per mouse. These statistical analyses were carried out using GraphPad Prism V5.00 (GraphPad Software, San Diego, California, USA). Statistical significance of the differences in tumor volume at day 10 (LLC) or day 9 (B16.F10) after the start of treatment was assessed by the Mann–Whitney *U*-test using the Statistical Software Package SPSS (SPSS Inc., Chicago, Illinois, USA). Differences were considered to be significant when the *P* value was less than 0.05, unless stated otherwise.

Results

Vandetanib treatment inhibited tumor growth in both Lewis lung carcinoma and B16.F10, but differentially affected vascular density

To investigate the molecular changes that occur in the tumor endothelium *in vivo* in a tumor that responds to antiangiogenic VEGFR2 inhibitor treatment, we treated LLC and B16.F10 tumor-bearing animals with the VEGFR2/EGFR tyrosine kinase inhibitor vandetanib at

a dose of 80 mg/kg daily. Treatment significantly inhibited LLC tumor growth and B16.F10 tumor growth by 84 and 82%, respectively (Fig. 1). In both tumor models, vascular morphology shifted upon treatment from large, irregularly shaped vessels to smaller vessels that were characterized by a more round and regular shape (Fig. 2a–d). However, a prominent difference between the two tumor models was observed in the vascular density after vandetanib treatment. Although in LLC the vascular density remained unaffected, a significant decrease in vascular density had occurred in B16.F10 tumors (Fig. 2e and f). Treatment significantly reduced the overall CD31-positive surface area of B16.F10 tumors by approximately 2-fold, which was confirmed by a 3-fold reduction in mRNA levels of the endothelial marker molecules CD31 and VE-cadherin in the tumor (Fig. 2g and h).

Vandetanib treatment differentially affected angiogene expression in Lewis lung carcinoma and B16.F10

As vascular density in LLC and B16.F10 tumors was differentially affected by vandetanib treatment, we hypothesized that vandetanib has a different effect on the underlying molecular behavior of the tumor endothelium in these two models. We thus compared the changes in expression of genes that are known to be involved in angiogenesis and vascular stabilization upon vandetanib treatment in the vasculature of LLC with those in B16.F10 vasculature.

VEGFR2/EGFR inhibitor therapy significantly downregulated mRNA expression of the proangiogenic/vascular destabilization molecules integrin β3 and Ang2 3-fold and significantly upregulated mRNA levels of the vascular stability molecules Tie2 and N-cadherin approximately 3-fold in LLC (Fig. 3). Furthermore, an approximately 1.5-fold decrease in PDGFRβ expression was observed in LLC tumor vasculature upon vandetanib treatment, as well as a 9-fold upregulation of desmin, which, however, did not reach statistical significance ($P = 0.08$) because of interindividual variation between the mice. In contrast, vandetanib treatment induced a 2.3-fold increase in eNOS mRNA in B16.F10 vasculature. In addition, PlGF showed a 3-fold downregulation upon vandetanib treatment, which did not reach statistical significance ($P = 0.09$). Although expression of integrin β3, PDGFRβ, and N-cadherin showed a similar, albeit nonsignificant, trend in B16.F10 compared with LLC, only P-selectin expression was similarly affected in both models, showing a significant more than 10-fold upregulation upon vandetanib treatment. The mRNA levels from all genes under study, as measured in the vasculature of both the vehicle- and vandetanib-treated groups of LLC and B16.F10 tumors, are depicted in Table 1.

Vandetanib treatment did not affect the overall pattern of pericyte coverage

As the genes that were most extensively affected by vandetanib treatment, such as Ang2, Tie2, and N-cadherin, play a (indirect) role in endothelial-pericyte adhesion, we hypothesized that vandetanib treatment increased coverage of the tumor vessels with pericytes. We therefore set out to study tumor vessel pericyte coverage in both LLC and B16.F10 by immunofluorescent double labeling for αSMA or desmin, together with CD31. The pattern of desmin coverage of LLC and B16.F10 blood vessels did not change upon vandetanib

Fig. 1

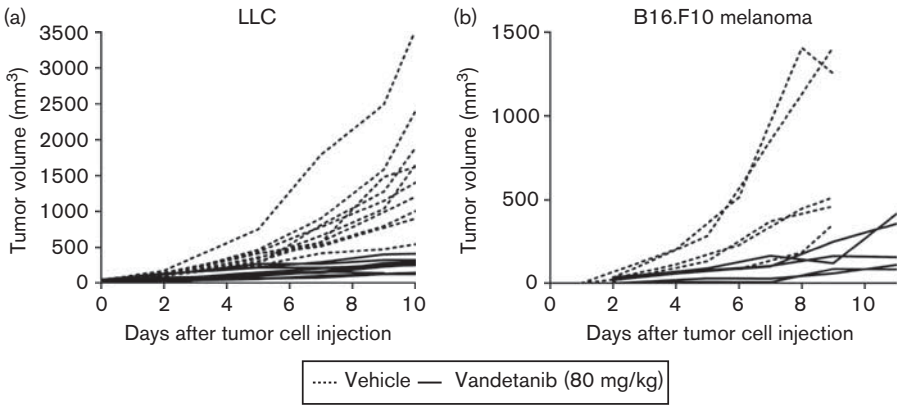

Vandetanib treatment significantly reduced outgrowth of Lewis lung carcinoma (LLC) and B16.F10 melanoma. (a and b) LLC-bearing and B16.F10-bearing mice were treated intraperitoneally on a daily basis with 80 mg/kg of the vascular endothelial growth factor receptor 2 inhibitor vandetanib in 5% arabic gum or with vehicle alone. Treatment was started when tumors appeared palpable and continued for 10 (LLC vehicle and vandetanib group), 9 (B16 vehicle group), or 11 (B16 vandetanib group) days. In the LLC model, treatment was omitted on the third and eighth day after the start of therapy. The graph represents tumor growth curves of each mouse (tumor) separately. The average tumor volumes in vandetanib-treated mice on day 10 (LLC) or day 9 (B16.F10) after the start of treatment were significantly smaller than those in vehicle-treated mice (the Mann–Whitney *U*-test; $P < 0.05$).

Fig. 2

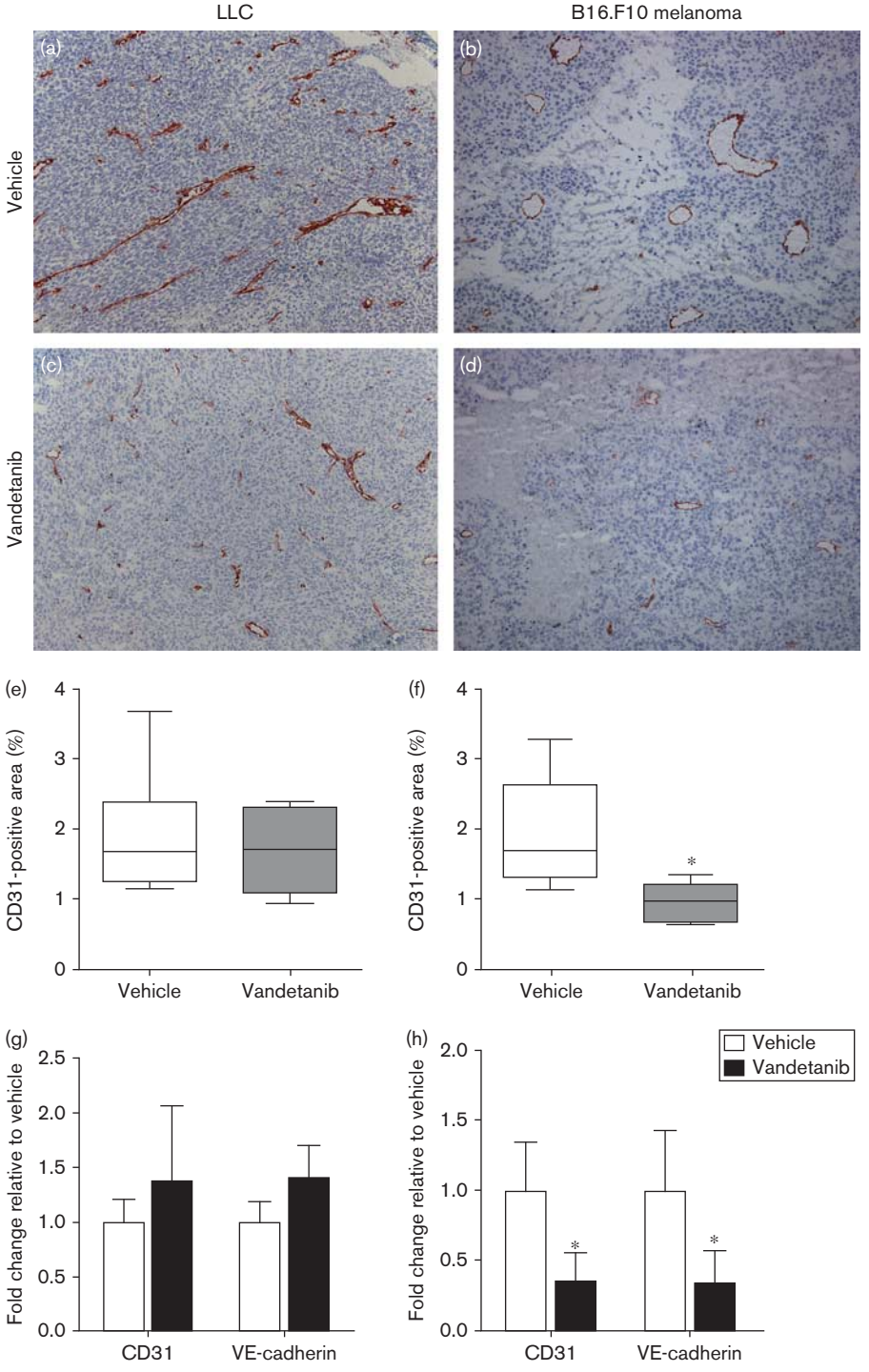

Vandetanib treatment reduced vascular surface area from B16.F10 melanoma, but not from Lewis lung carcinoma (LLC). (a–d) Vascular morphology of vandetanib and vehicle-treated LLC and B16.F10 tumors. Immunohistochemical staining for CD31, magnification ×100. (e and f) Quantification of CD31-positive surface area in tumor sections using morphometric analysis. Graph represents median of six (LLC) or five (B16) tumors, minimum and maximum. (g and h) mRNA levels of endothelial marker genes CD31 and VE-cadherin in B16.F10 and LLC tumors of vandetanib and vehicle-treated mice, normalized to GAPDH. Values represent mean of duplicate quantitative reverse transcriptase polymerase chain reaction analysis of six (LLC) or five (B16.F10) animals per group. *$P<0.05$ versus vehicle-treated control.

Fig. 3

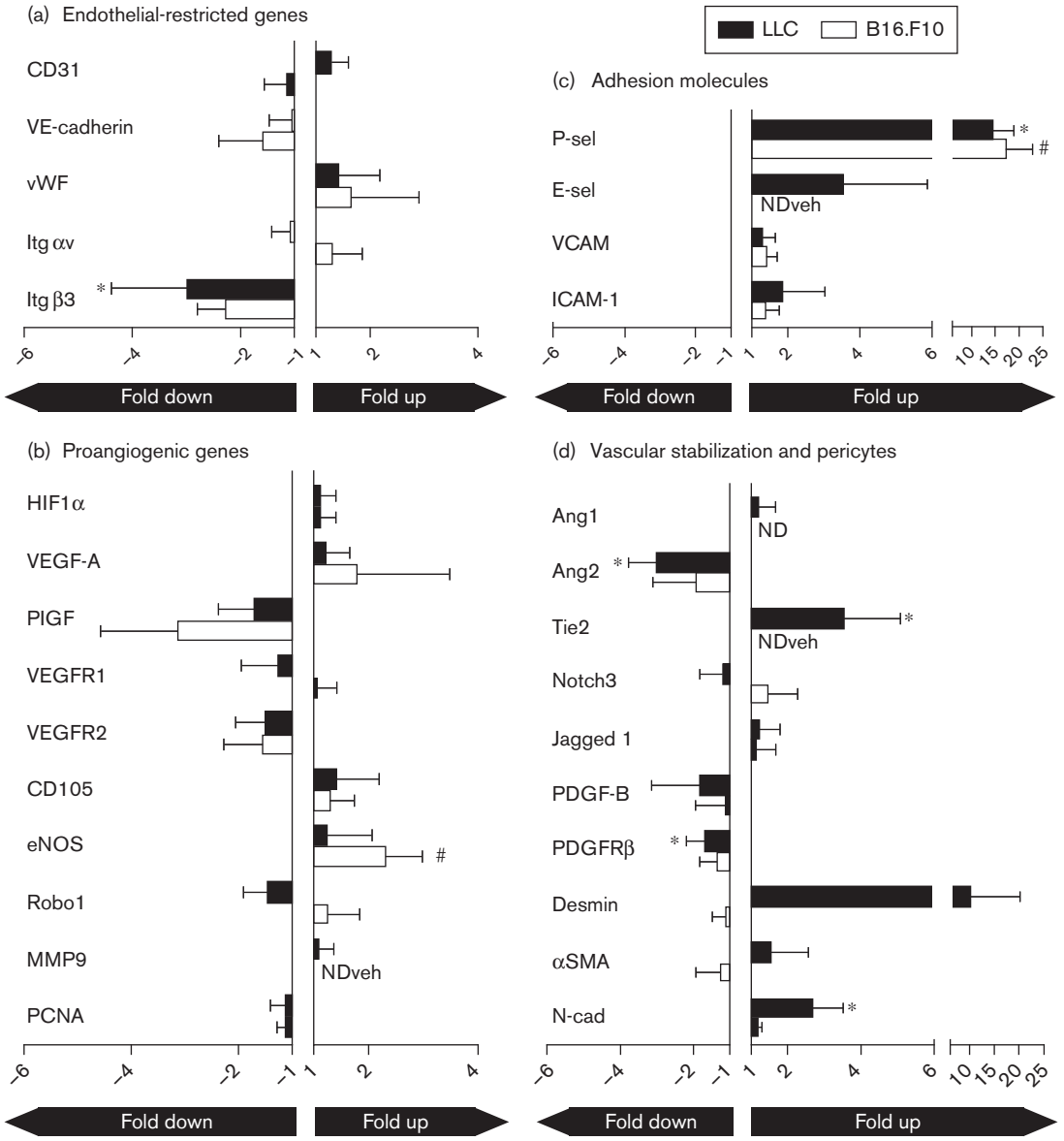

Vandetanib-induced changes in gene expression in Lewis lung carcinoma (LLC) and B16.F10 tumor vasculature. (a–d) mRNA expression levels of various angiogenesis-associated and vascular behavior-determining genes in tumor vasculature that was isolated by laser microdissection from LLC and B16.F10 tumors treated with vandetanib or vehicle alone. Values represent fold increase or decrease in mRNA expression in the vasculature of vandetanib-treated tumors compared with vehicle-treated tumors, normalized to GAPDH. Mean + SD of six (LLC) or five (B16.F10) animals per group. NDveh, not detectable in vehicle-treated mice, no ratio could be calculated. ND, not detectable in both vehicle-treated and vandetanib-treated groups. *$P<0.05$ versus vehicle-treated control in LLC. #$P<0.05$ versus vehicle-treated control in B16.F10.

treatment (Fig. 4). The expression of αSMA was much more heterogenously distributed throughout the tumors of both types compared with desmin expression. Not only was αSMA restricted to the merely lumen-containing large vessels, but also the intensity of the staining largely varied between blood vessels. Quantification revealed that the percentage of αSMA-positive vessels was not changed by treatment in either of the two tumor models (data not shown). Furthermore, we found that, in general, B16.F10 tumor vessels were more intensely covered by αSMA-positive pericytes than were LLC vessels (Fig. 4; data not shown).

Vandetanib-induced loss of target protein expression is not posttranslationally controlled by miR-296

As vascular density was differentially affected by vandetanib in LLC and B16.F10 tumors, we hypothesized that the drug may target different compartments within the tumor in these two models. We therefore assessed the localization of the drug's main target receptors. In

Table 1 mRNA levels adjusted to GAPDH (× 1000) of angiogenesis and vascular behavior-assoicated genes in tumor vasculature from vehicle and vandetanib-treated tumors

	B16.F10 melanoma		Lewis lung carcinoma	
Gene	Vehicle	Vandetanib	Vehicle	Vandetanib
CD31	6.40 ± 3.26	5.79 ± 2.34	109.16 ± 16.22	133.07 ± 40.42
VEcad	5.33 ± 4.36	3.16 ± 2.13	165.95 ± 72.60	169.18 ± 53.22
vWF	1.65 ± 0.71	2.67 ± 2.12	66.33 ± 40.42	89.93 ± 54.54
Itgαv	1.06 ± 0.31	1.36 ± 0.60	22.95 ± 6.93	22.36 ± 8.69
Itgβ3	0.96 ± 0.76	0.42 ± 0.10	46.88 ± 17.76	15.91 ± 7.76
HIF1α	3.48 ± 1.19	3.79 ± 1.09	32.66 ± 20.46	35.36 ± 10.43
VEGF-A	0.77 ± 0.24	1.37 ± 1.31	42.95 ± 10.31	50.59 ± 20.70
PlGF	1.61 ± 1.46	0.52 ± 0.24	8.11 ± 4.02	4.89 ± 2.09
VEGFR1	0.66 ± 0.40	0.67 ± 0.27	27.03 ± 6.79	22.12 ± 12.99
VEGFR2	1.17 ± 0.97	0.76 ± 0.36	72.96 ± 20.07	50.05 ± 20.32
CD105	9.09 ± 2.75	11.52 ± 4.28	85.64 ± 58.69	120.25 ± 69.03
eNOS	0.26 ± 0.07	0.61 ± 0.18	10.60 ± 4.88	12.86 ± 9.12
Robo1	0.18 ± 0.07	0.23 ± 0.11	1.00 ± 0.20	0.71 ± 0.25
MMP9	Not determined	0.15 ± 0.03	22.67 ± 17.75	24.01 ± 7.28
PCNA	23.53 ± 4.85	21.62 ± 4.16	24.13 ± 10.28	21.85 ± 5.92
Ang1	Not determined	Not determined	1.27 ± 0.83	1.43 ± 0.69
Ang2	1.12 ± 0.57	0.58 ± 0.36	30.05 ± 5.81	10.09 ± 2.70
Tie2	Not determined	0.57 ± 0.35	3.68 ± 1.60	12.78 ± 5.89
Notch3	0.68 ± 0.39	0.98 ± 0.57	7.79 ± 3.83	7.05 ± 4.65
Jag1	1.02 ± 0.59	1.08 ± 0.62	38.72 ± 7.32	46.13 ± 23.13
PDGF-B	3.67 ± 2.43	3.49 ± 2.95	62.32 ± 22.85	35.56 ± 28.45
PDGF-Rβ	1.40 ± 0.61	1.08 ± 0.44	43.41 ± 9.72	26.50 ± 9.00
Desmin	0.15 ± 0.08	0.14 ± 0.05	0.63 ± 0.22	4.61 ± 5.75
αSMA	16.50 ± 6.21	13.35 ± 7.49	28.61 ± 10.06	42.45 ± 31.00
N-cad	3.93 ± 1.13	4.48 ± 0.60	1.54 ± 0.69	4.50 ± 1.34
P-sel	0.21 ± 0.17	3.53 ± 1.25	1.27 ± 0.63	17.84 ± 6.22
E-sel	Not determined	0.65 ± 0.10	0.73 ± 0.01	2.53 ± 1.77
VCAM-1	0.28 ± 0.07	0.37 ± 0.10	67.87 ± 22.36	82.95 ± 28.83
ICAM-1	0.61 ± 0.38	0.83 ± 0.25	7.47 ± 2.02	13.20 ± 9.30

both tumor models, expression of VEGFR2 was restricted to the endothelium and covered the full vasculature of the tumor before the start of vandetanib treatment. Strikingly, VEGFR2 staining was strongly diminished after treatment in both LLC and B16.F10 tumors (Fig. 5a–l). As a part of vandetanib's pharmacological activity can be attributed to EGFR inhibitory activity, we analyzed the localization of EGFR expression. The observation that EGFR expression is restricted to the vasculature (Fig. 5a–l) implies that, in the two tumor models studied, vandetanib selectively targeted the tumor blood vessels. In contrast to VEGFR2, EGFR was expressed only in a subset of the vasculature, predominantly on lumen-containing vessels, whereas smaller vascular structures were devoid of expression. Vandetanib treatment also reduced EGFR expression, although this reduction was less pronounced than for VEGFR2.

Interestingly, although protein levels of these target receptors decreased, their mRNA levels remained unaffected in LLC and B16.F10 tumor vasculature (Fig. 5m and n). This difference between RNA and protein suggests that the observed downregulation of VEGFR2 upon therapy might be the result of posttranslational regulation. Recently, Wurdinger *et al.* [22] reported that microRNA miR-296 can control VEGFR2 protein expression. Angiogenic growth factors have been demonstrated to increase the level of miR-296, which in turn increases protein expression of VEGFR2. To assess whether a change in miR-296 levels is associated with the vandetanib-induced loss of VEGFR2 protein expression observed in both of our tumor models, we analyzed expression levels of miR-296 in whole tumor samples from LLC and B16.F10 tumors and in microdissected B16.F10 tumor vasculature. We corrected for the amount of endothelium in our sample by including the endothelium-restricted miR-126. Vandetanib treatment did not change the expression levels of miR-296 in LLC and B16.F10 tumors, nor in microdissected B16.F10 tumor vasculature (Fig. 6), suggesting that the vandetanib-induced downregulation of VEGFR2 protein is not posttranslationally controlled by miR-296.

Discussion

The first direct clinical evidence that anti-VEGF therapy exerts antivascular effects came from the landmark study by Willett *et al.* [23], who demonstrated that bevacizumab treatment together with chemotherapy reduced tumor vascular density and blood flow, interstitial fluid pressure, and the number of viable circulating endothelial progenitor cells in patients with advanced rectal cancer. Despite a few clinical successes, VEGFR2-specific inhibitors have shown little activity in solid tumors when used as a monotherapy in the clinic [6]. Importantly, the molecular events that orchestrate the above-mentioned cellular effects of antiangiogenic therapy have been poorly understood until now, and their contribution to successful antitumor effects in the preclinical setting remains unclear. In this study we demonstrate that efficient tumor growth inhibition induced by vandetanib treatment is accompanied by a significant decrease in microvascular density in B16.F10 tumors. In contrast, vandetanib treatment induced a similar degree of tumor growth inhibition in LLC, leaving vascular density unaffected. Although vandetanib treatment downregulated expression of the proangiogenic genes integrin β3 and Ang2, and upregulated the expression of the vascular stability molecules Tie2 and N-cadherin in LLC vasculature, thereby inducing a shift toward vascular stabilization, none of these genes were significantly affected in B16.F10 vasculature. In contrast, B16.F10 vasculature exhibited increased expression of eNOS upon treatment. This suggests that vandetanib exerts its antitumor effect in LCC by inhibition of angiogenic sprouting and by promoting a more stabilized vascular phenotype, whereas in B16.F10 other molecular changes play a role in creating the antitumor effect observed. Interestingly, in neither LLC nor B16.F10, was the pattern of pericyte coverage significantly altered by vandetanib treatment. As in both LLC and B16.F10, VEGFR2 and EGFR were restricted to the vasculature, our data indicate that pharmacologically targeting the vasculature alone can exert a potent antitumor effect. Moreover, the observation that VEGFR2 was more intensely expressed by the vasculature than was

Fig. 4

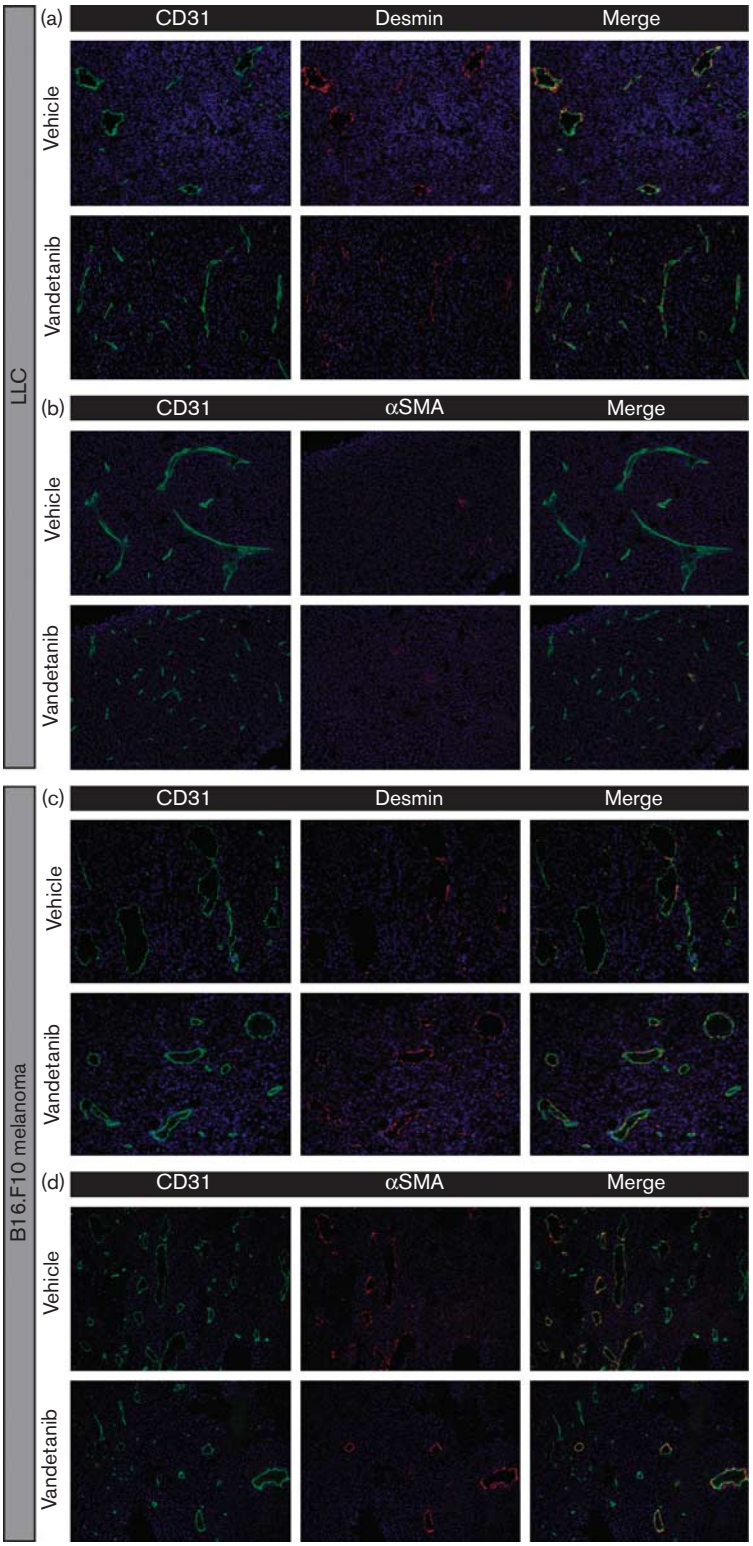

Vandetanib does not affect the pattern of pericyte coverage in Lewis lung carcinoma (LLC) and B16.F10. Immunofluorescent double staining for CD31 (green) and desmin (red) or αSMA (red) and nuclear counterstain (DAPI; blue) from a representative LLC tumor (a and b) and B16.F10 tumor (c and d). Magnification ×200 for desmin staining and ×100 for αSMA staining.

Fig. 5

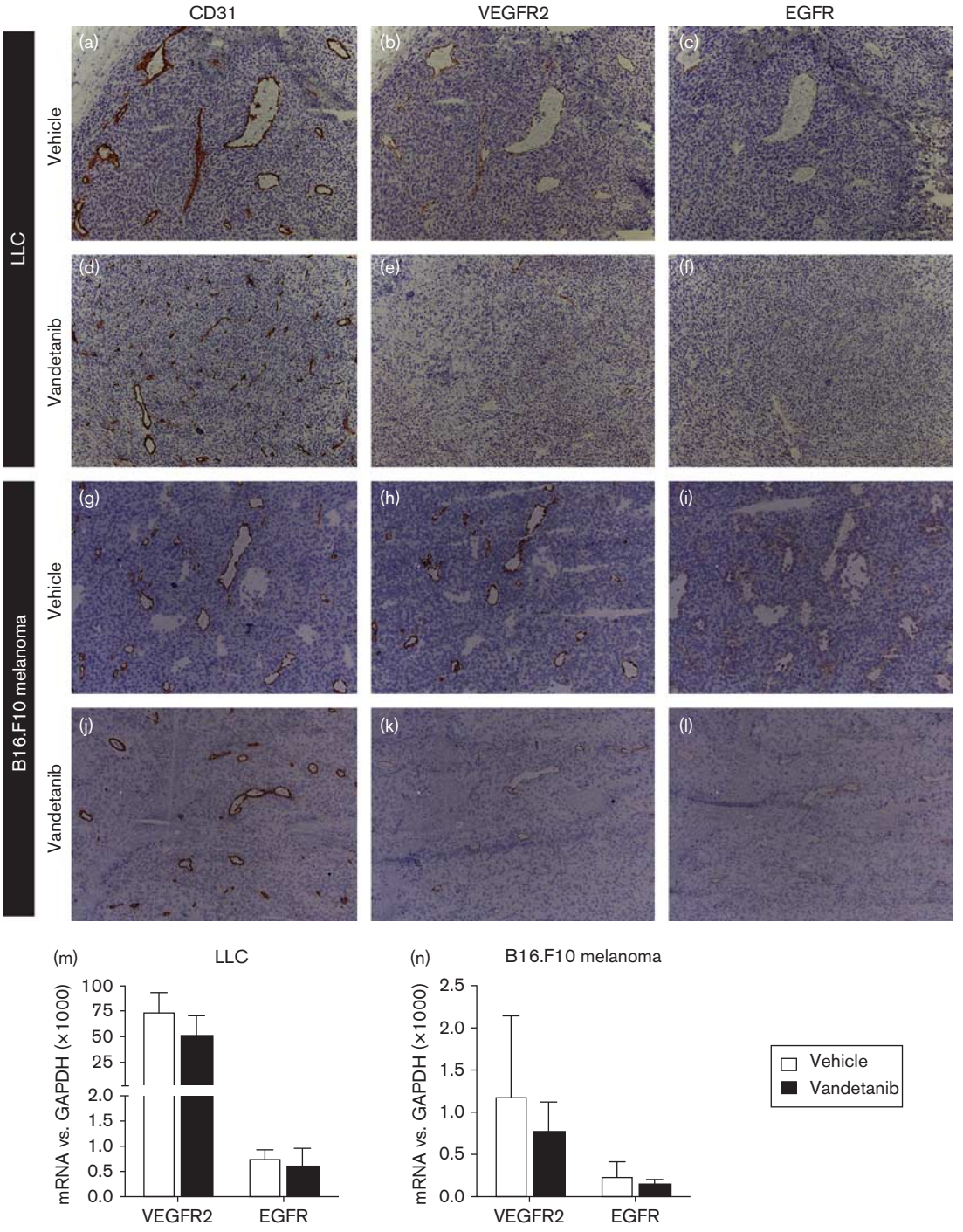

Pharmacological targeting of vascular endothelial growth factor receptor 2 (VEGFR2)/epidermal growth factor receptor (EGFR) with vandetanib resulted in downregulation of the target receptors at the protein level, whereas mRNA remained unaffected. (a–l) Protein expression of both VEGFR2 and EGFR was significantly reduced after treatment in Lewis lung carcinoma (LLC; a–f) and B16.F10 (g–l), as visualized by immunohistochemical staining of consecutive sections for VEGFR2, EGFR, and CD31; magnification ×100. Interstitial dermal cells and some vessels in the skin surrounding the tumor strongly stained for EGFR, representing a good internal positive control (not shown). (m and n) mRNA levels of VEGFR2 and EGFR in microdissected tumor vasculature from LLC (M) and B16.F10 (N) tumors. Values represent mean of duplicate quantitative reverse transcriptase polymerase chain reaction analysis + SD of six (LLC) or five (B16) animals per group.

Fig. 6

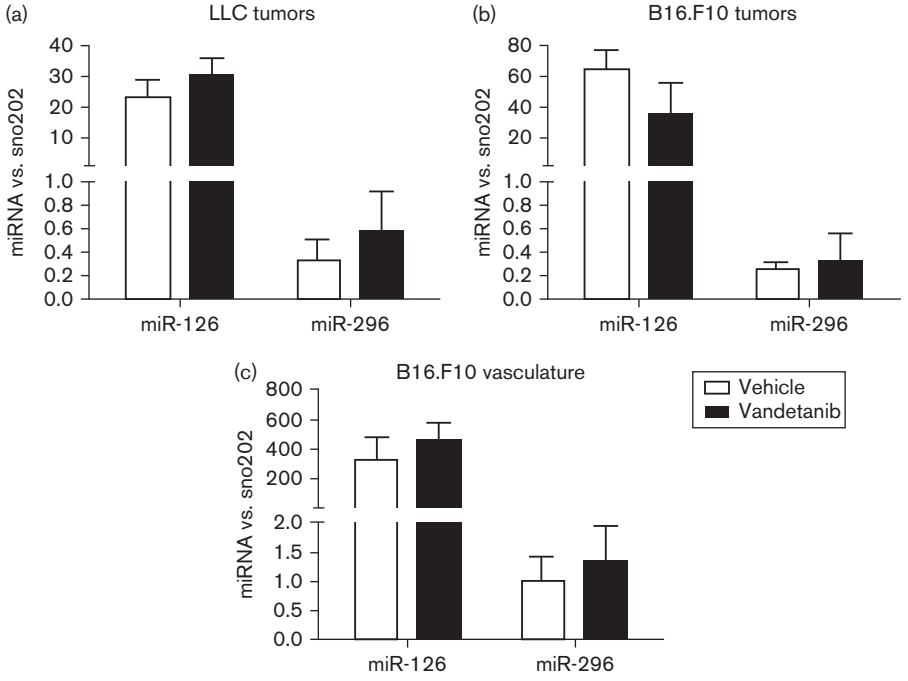

The downregulation of vascular endothelial growth factor receptor 2 (VEGFR2) protein was not related to microRNA-296 expression. Vandetanib treatment did not affect miR-296 expression levels in the Lewis lung carcinoma (LLC; a) and B16.F10 (b) tumor as a whole, nor in B16.F10 tumor vasculature isolated by laser microdissection before quantitative reverse transcriptase polymerase chain reaction analysis (c). Values represent miR-296 expression levels normalized to the small nuclear RNA sno-202, mean of triplicate qRT-PCR analysis of six (LLC) or five (B16) animals per group. The endothelial-restricted miR-126 was included as control.

EGFR, together with the fact that vandetanib has a 10-fold higher affinity for VEGFR2 than for EGFR [18], implies that the observed effects of vandetanib are mediated by VEGFR2 inhibition. The vandetanib-induced loss of VEGFR2 protein expression, which was not related to changes in miR-296 expression, requires further studies, as it may severely hamper therapeutic efficacy when longer time periods of treatment are required.

The results of our study suggest that pharmacological targeting of the vasculature alone can induce a potent antitumor effect, and as such supports the observation previously published by Mavria and Porter [24]. They showed that selective transduction of proliferating endothelium with thymidine kinase followed by gangciclovir treatment inhibited tumor growth of KS Y-1 xenografts just as efficiently as selectively targeting the tumor cell compartment [24]. Our study demonstrated that effective tumor growth inhibition by targeting the vasculature alone does not *per se* coincide with a reduced overall vascular surface area, and that the effect of the drug on this parameter is highly dependent on the tumor type under study. Our data confirm previous reports that vessel density does not necessarily associate with antiangiogenic efficacy [25–27], although the majority of preclinical studies with small molecule VEGFR2 tyrosine kinase inhibitors have related efficient tumor growth inhibition by targeting the vasculature to a reduction in tumor vascular density [7,9,28].

Vandetanib-induced inhibition of LLC tumor growth was accompanied by a significant decrease in the expression of the integrin subunit β3. Two independent studies have demonstrated that angiogenic activation of endothelial cells is characterized by an elevated expression of this molecule [14,29], and thus its loss may be indicative of a reduction in angiogenic activity. Moreover, vandetanib treatment downregulated the expression of Ang2 and upregulated the expression of Tie2 in LLC endothelium, which points to a shift in Ang1/Ang2/Tie2 balance toward Ang1-Tie2-driven vascular stabilization [30]. This suggests that vandetanib exerts its antitumor effect in this specific tumor model by inhibiting angiogenic sprouting and promoting a more stabilized vascular phenotype. An initiating molecular mechanism to facilitate the occurrence of vascular stabilization under pharmacological pressure of a VEGFR2 inhibitor is that prevention of VEGFR2 signaling inhibits the assembly of a complex consisting of VEGFR2 and PDGFRβ on pericytes, thereby disabling VEGF/VEGFR2 induced inhibition of endothelial-pericyte attachment [31]. Hence, VEGFR2 inhibition increased pericyte coverage and tumor vessel maturation [25,32–34]. Once vessels are matured, they

may lose their dependency on VEGF and thus their sensitivity for VEGFR2 inhibition during the course of therapy [33], as also suggested by the observed loss of VEGFR2 protein. Although our data did not reveal a change in the number of pericytes covering the vasculature per se, the enhanced degree of vascular stabilization strengthens the concept that more efficient antiangiogenic therapy should target both endothelial cells and pericytes [35]. In light of the loss of target protein, future studies should validate whether VEGFR2 inhibitor-induced loss of the target receptor occurs in human cancers, to evaluate the use of VEGFR2 as a target of choice. This emphasizes the need for tumor biopsies from patients treated with anti-VEGF therapy, ideally at different time points after treatment.

Our data in LLC indicate that VEGFR2/EGFR inhibition through vandetanib slows down tumor growth by inhibition of angiogenic sprouting and by promoting a more stabilized and quiescent vascular phenotype. These findings fit the current hypothesis that VEGFR2 inhibitor treatment restores the balance between proangiogenic and antiangiogenic signaling by inactivating the surplus of VEGF activity. Normalization of this balance would result in a more regular vascular morphology, improved blood flow, and reduced vascular permeability, thereby reducing the elevated interstitial pressure and facilitating uptake of, for example, chemotherapeutic agents into the tumor tissue [36,37]. Importantly, several aspects of vascular normalization, such as a decrease in vascular diameter, require activation of Tie2 through Ang1 [38]. The observed upregulation of Tie2 mRNA, and downregulation of mRNA of its antagonist Ang2, suggests enhanced signaling of Tie2, which would thus contribute to vandetanib-induced vascular normalization.

Although gene expression in the LLC showed a clear shift toward stabilization upon vandetanib treatment, B16.F10 vasculature responded to vandetanib only by upregulating eNOS and P-selectin. This demonstrates that, although the outcome of therapy can be the same, the underlying molecular changes that orchestrate the antitumor effect differ between tumor types. It is likely that human tumors will respond to therapy with an even larger degree of heterogeneity, emphasizing that successful evaluation of the therapeutic efficacy of antiangiogenic treatment will require identification and validation of specific biomarkers for each type of tumor [39].

A striking observation in both tumor models was the loss of VEGFR2 protein expression upon vandetanib treatment, whereas VEGFR2 mRNA levels in the vasculature remained unaffected. This suggested a role for post-translational modification of growth factor receptor expression. Recently, Wurdinger *et al.* [22] demonstrated that microRNA-296 indirectly regulates expression of VEGFR2 by inhibiting the translation of hepatocyte growth factor-regulated tyrosine kinase substrate (HGS), a protein that is involved in targeted degradation of VEGFR2. Importantly, in this system, expression of miR-296 was upregulated by VEGF signaling through VEGFR2 in human brain microvascular endothelial cells co-cultured with glioma cells. The administration of antagomirs to miR-296 to mice bearing U87 tumors reduced neovascularization, and in clinical glioblastoma specimens the increased miR-296 expression was associated with elevated VEGFR2 protein levels in the vasculature [22]. We thus hypothesized that blockade of VEGF signaling upon vandetanib treatment would reduce the expression of miR-296, thereby leading to enhanced degradation of VEGFR2 protein. Our data, however, demonstrated that a role for miR-296 in the vandetanib-induced loss of VEGFR2 in these two tumor models could be excluded. Other explanations for the loss of VEGFR2 protein include inhibition of VEGF-activated recycling of VEGFR2 to the membrane by vandetanib [40] or the involvement of a hypoxia-induced decline in VEGFR2 protein levels [41], as a result of inhibition of neovascularization by the drug. As this was not the aim of our study, we did not investigate these possibilities in more detail.

In summary, we demonstrated that vandetanib treatment inhibits tumor growth by interfering with different molecular processes in LLC compared with B16.F10, even though the pharmacological target is, in both models, present in the same compartment – that is, in the vasculature. Furthermore, we demonstrated that vandetanib treatment induced loss of VEGFR2 protein expression, which had no relation to the VEGFR2-controlling microRNA-296 recently reported in glioma vasculature. Future studies should focus on validation of our observations in human tumor biopsies, and, where possible, extension thereof by genome-wide transcriptional analyses and kinome profiling [42–44], for which proper clinical specimens are an essential prerequisite. Importantly, in these studies, each tumor type and each tumor in its own location should be appreciated by its own merits [45]. Such knowledge will contribute to a complete understanding of the molecular effects of antiangiogenic therapy and their relation to creating a successful antitumor effect in the clinic.

Acknowledgements

The authors thank Anita Meter-Arkema for excellent technical assistance and M. Schipper for excellent morphometrical analysis, and also thank AstraZeneca (Macclesfield, UK) for the generous gift of vandetanib.

Source of funding: This research was funded by the University of Groningen.

Conflicts of interest

There are no conflicts of interest.

References

1 Dvorak HF. Vascular permeability factor/vascular endothelial growth factor: a critical cytokine in tumor angiogenesis and a potential target for diagnosis and therapy. *J Clin Oncol* 2002; **20**:4368–4380.

2 Pettersson A, Nagy JA, Brown LF, Sundberg C, Morgan E, Jungles S, *et al*. Heterogeneity of the angiogenic response induced in different normal adult tissues by vascular permeability factor/vascular endothelial growth factor. *Lab Invest* 2000; **80**:99–115.

3 Jain RK, Duda DG, Clark JW, Loeffler JS. Lessons from phase III clinical trials on anti-VEGF therapy for cancer. *Nat Clin Pract Oncol* 2006; **3**: 24–40.

4 Folkman J. Angiogenesis: an organizing principle for drug discovery? *Nat Rev Drug Discov* 2007; **6**:273–286.

5 Ellis LM, Hicklin DJ. VEGF-targeted therapy: mechanisms of anti-tumour activity. *Nat Rev Cancer* 2008; **8**:579–591.

6 Duda DG, Batchelor TT, Willett CG, Jain RK. VEGF-targeted cancer therapy strategies: current progress, hurdles and future prospects. *Trends Mol Med* 2007; **13**:223–230.

7 Wedge SR, Ogilvie DJ, Dukes M, Kendrew J, Chester R, Jackson JA, *et al*. ZD6474 inhibits vascular endothelial growth factor signaling, angiogenesis, and tumor growth following oral administration. *Cancer Res* 2002; **62**:4645–4655.

8 Laird AD, Vajkoczy P, Shawver LK, Thurnher A, Liang C, Mohammadi M, *et al*. SU6668 is a potent antiangiogenic and antitumor agent that induces regression of established tumors. *Cancer Res* 2000; **60**:4152–4160.

9 Sasaki T, Kitadai Y, Nakamura T, Kim JS, Tsan RZ, Kuwai T, *et al*. Inhibition of epidermal growth factor receptor and vascular endothelial growth factor receptor phosphorylation on tumor-associated endothelial cells leads to treatment of orthotopic human colon cancer in nude mice. *Neoplasia* 2007; **9**:1066–1077.

10 Witmer AN, Van Blijswijk BC, Van Noorden CJ, Vrensen GF, Schlingemann RO. In-vivo angiogenic phenotype of endothelial cells and pericytes induced by vascular endothelial growth factor-A. *J Histochem Cytochem* 2004; **52**:39–52.

11 Hicklin DJ, Ellis LM. Role of the vascular endothelial growth factor pathway in tumor growth and angiogenesis. *J Clin Oncol* 2005; **23**:1011–1027.

12 Suehiro J, Hamakubo T, Kodama T, Aird WC, Minami T. Vascular endothelial growth factor activation of endothelial cells is mediated by early growth response-3. *Blood* 2010; **115**:2520–2532.

13 Zeng H, Qin L, Zhao D, Tan X, Manseau EJ, Van Hoang M, *et al*. Orphan nuclear receptor TR3/Nur77 regulates VEGF-A-induced angiogenesis through its transcriptional activity. *J Exp Med* 2006; **203**:719–729.

14 Abdollahi A, Schwager C, Kleeff J, Esposito I, Domhan S, Peschke P, *et al*. Transcriptional network governing the angiogenic switch in human pancreatic cancer. *Proc Natl Acad Sci USA* 2007; **104**:12890–12895.

15 Holderfield MT, Hughes CC. Crosstalk between vascular endothelial growth factor, notch, and transforming growth factor-beta in vascular morphogenesis. *Circ Res* 2008; **102**:637–652.

16 Dirkx AE, Oude Egbrink MG, Kuijpers MJ, Van der Niet ST, Heijnen VV, Bouma-ter Steege JC, *et al*. Tumor angiogenesis modulates leukocyte-vessel wall interactions *in vivo* by reducing endothelial adhesion molecule expression. *Cancer Res* 2003; **63**:2322–2329.

17 Hennequin LF, Stokes ES, Thomas AP, Johnstone C, Ple PA, Ogilvie DJ, *et al*. Novel 4-anilinoquinazolines with C-7 basic side chains: design and structure activity relationship of a series of potent, orally active, VEGF receptor tyrosine kinase inhibitors. *J Med Chem* 2002; **45**: 1300–1312.

18 Ryan AJ, Wedge SR. ZD6474: a novel inhibitor of VEGFR and EGFR tyrosine kinase activity. *Br J Cancer* 2005; **92 (Suppl 1):**S6–S13.

19 Morabito A, Piccirillo MC, Falasconi F, De FG, Del GA, Bryce J, *et al*. Vandetanib (ZD6474), a dual inhibitor of vascular endothelial growth factor receptor (VEGFR) and epidermal growth factor receptor (EGFR) tyrosine kinases: current status and future directions. *Oncologist* 2009; **14**: 378–390.

20 Wagemakers M, Van der Wal GE, Cuberes R, Alvarez I, Andres EM, Buxens J, *et al*. COX-2 inhibition combined with radiation reduces orthotopic glioma outgrowth by targeting the tumor vasculature. *Transl Oncol* 2009; **2**:1–7.

21 Kuldo JM, Westra J, Asgeirsdottir SA, Kok RJ, Oosterhuis K, Rots MG, *et al*. Differential effects of NF-{kappa}B and p38 MAPK inhibitors and combinations thereof on TNF-{alpha}- and IL-1{beta}-induced proinflammatory status of endothelial cells *in vitro*. *Am J Physiol Cell Physiol* 2005; **289**:C1229–C1239.

22 Wurdinger T, Tannous BA, Saydam O, Skog J, Grau S, Soutschek J, *et al*. miR-296 regulates growth factor receptor overexpression in angiogenic endothelial cells. *Cancer Cell* 2008; **14**:382–393.

23 Willett CG, Boucher Y, di TE, Duda DG, Munn LL, Tong RT, *et al*. Direct evidence that the VEGF-specific antibody bevacizumab has antivascular effects in human rectal cancer. *Nat Med* 2004; **10**:145–147.

24 Mavria G, Porter CD. Reduced growth in response to ganciclovir treatment of subcutaneous xenografts expressing HSV-tk in the vascular compartment. *Gene Ther* 2001; **8**:913–920.

25 Cesca M, Frapolli R, Berndt A, Scarlato V, Richter P, Kosmehl H, *et al*. The effects of vandetanib on paclitaxel tumor distribution and antitumor activity in a xenograft model of human ovarian carcinoma. *Neoplasia* 2009; **11**: 1155–1164.

26 Hlatky L, Hahnfeldt P, Folkman J. Clinical application of antiangiogenic therapy: microvessel density, what it does and doesn't tell us. *J Natl Cancer Inst* 2002; **94**:883–893.

27 Sandstrom M, Johansson M, Andersson U, Bergh A, Bergenheim AT, Henriksson R. The tyrosine kinase inhibitor ZD6474 inhibits tumour growth in an intracerebral rat glioma model. *Br J Cancer* 2004; **91**:1174–1180.

28 Eichhorn ME, Strieth S, Luedemann S, Kleespies A, Noth U, Passon A, *et al*. Contrast enhanced MRI and intravital fluorescence microscopy indicate improved tumor microcirculation in highly vascularized melanomas upon short-term anti-VEGFR treatment. *Cancer Biol Ther* 2008; **7**:1006–1013.

29 Palmowski M, Huppert J, Ladewig G, Hauff P, Reinhardt M, Mueller MM, *et al*. Molecular profiling of angiogenesis with targeted ultrasound imaging: early assessment of antiangiogenic therapy effects. *Mol Cancer Ther* 2008; **7**:101–109.

30 Augustin HG, Koh GY, Thurston G, Alitalo K. Control of vascular morphogenesis and homeostasis through the angiopoietin-Tie system. *Nat Rev Mol Cell Biol* 2009; **10**:165–177.

31 Greenberg JI, Shields DJ, Barillas SG, Acevedo LM, Murphy E, Huang J, *et al*. A role for VEGF as a negative regulator of pericyte function and vessel maturation. *Nature* 2008; **456**:809–813.

32 Vecchiarelli-Federico LM, Cervi D, Haeri M, Li Y, Nagy A, Ben-David Y. Vascular endothelial growth factor: a positive and negative regulator of tumor growth. *Cancer Res* 2010; **70**:863–867.

33 Helfrich I, Scheffrahn I, Bartling S, Weis J, von Felbert V, Middleton M, *et al*. Resistance to antiangiogenic therapy is directed by vascular phenotype, vessel stabilization, and maturation in malignant melanoma. *J Exp Med* 2010; **207**:491–503.

34 Palmowski M, Huppert J, Hauff P, Reinhardt M, Schreiner K, Socher MA, *et al*. Vessel fractions in tumor xenografts depicted by flow- or contrast-sensitive three-dimensional high-frequency Doppler ultrasound respond differently to antiangiogenic treatment. *Cancer Res* 2008; **68**:7042–7049.

35 Bergers G, Song S, Meyer-Morse N, Bergsland E, Hanahan D. Benefits of targeting both pericytes and endothelial cells in the tumor vasculature with kinase inhibitors. *J Clin Invest* 2003; **111**:1287–1295.

36 Jain RK. Normalization of tumor vasculature: an emerging concept in antiangiogenic therapy. *Science* 2005; **307**:58–62.

37 Claes A, Leenders W. Vessel normalization by VEGF inhibition: a complex story. *Cancer Biol Ther* 2008; **7**:1014–1016.

38 Winkler F, Kozin SV, Tong RT, Chae SS, Booth MF, Garkavtsev I, *et al*. Kinetics of vascular normalization by VEGFR2 blockade governs brain tumor response to radiation: role of oxygenation, angiopoietin-1, and matrix metalloproteinases. *Cancer Cell* 2004; **6**:553–563.

39 Hanrahan EO, Lin HY, Kim ES, Yan S, Du DZ, McKee KS, *et al*. Distinct patterns of cytokine and angiogenic factor modulation and markers of benefit for vandetanib and/or chemotherapy in patients with non-small-cell lung cancer. *J Clin Oncol* 2010; **28**:193–201.

40 Gampel A, Moss L, Jones MC, Brunton V, Norman JC, Mellor H. VEGF regulates the mobilization of VEGFR2/KDR from an intracellular endothelial storage compartment. *Blood* 2006; **108**:2624–2631.

41 Olszewska-Pazdrak B, Hein TW, Olszewska P, Carney DH. Chronic hypoxia attenuates VEGF signaling and angiogenic responses by downregulation of KDR in human endothelial cells. *Am J Physiol Cell Physiol* 2009; **296**:C1162–C1170.

42 Stockwin LH, Vistica DT, Kenney S, Schrump DS, Butcher DO, Raffeld M, *et al*. Gene expression profiling of alveolar soft-part sarcoma (ASPS). *BMC Cancer* 2009; **9**:22.

43 Buckanovich RJ, Sasaroli D, O'Brien-Jenkins A, Botbyl J, Hammond R, Katsaros D, *et al*. Tumor vascular proteins as biomarkers in ovarian cancer. *J Clin Oncol* 2007; **25**:852–861.

44 Sikkema AH, Diks SH, den Dunnen WF, ter Elst A, Scherpen FJ, Hoving EW, *et al*. Kinome profiling in pediatric brain tumors as a new approach for target discovery. *Cancer Res* 2009; **69**:5987–5995.

45 Langenkamp E, Molema G. Microvascular endothelial cell heterogeneity: general concepts and pharmacological consequences for anti-angiogenic therapy of cancer. *Cell Tissue Res* 2009; **335**:205–222.